Date July 2010
Author Renzsch, H.F. and K. Graf

Address Delft University of Technology
Ship Hydromechanics Laboratory
Mekelweg 2, 2628 CD Delft

Delft University of Technology

Fluid structure interaction simulation of Spinnakers – Getting closer to reality

by

H.F. Renzsch and K. Graf

Report No. 1686-P **2010**

Published in: Proceedings of the 2nd International Conference on Innovation in High Performance Sailing Yachts, 30 June – 1 July 2010, Lorient, France, Royal Institution of Naval Architects, RINA, ISBN: 978-1-905040-72-8

THE SECOND INTERNATIONAL CONFERENCE ON INNOVATION IN HIGH PERFORMANCE SAILING YACHTS

30 June - 1 July 2010, Lorient, France

PAPERS

Sponsored by:

esi get it right®

ANSYS®

THE ROYAL INSTITUTION OF NAVAL ARCHITECTS
10 UPPER BELGRAVE STREET, LONDON, SW1X 8BQ Telephone: +44 (0)20 7235 4622

RINA

THE SECOND INTERNATIONAL CONFERENCE ON INNOVATION IN HIGH PERFORMANCE SAILING YACHTS

30 June – 1 July 2010

THE ROYAL INSTITUTION OF NAVAL ARCHITECTS
10 Upper Belgrave Street
London SW1X 8BQ

Telephone: 020 7235 4622
Fax: 020 7259 5912

ISBN No: 978-1-905040-72-8

CONTENTS

* - Not available at time of printing

FLUID STRUCTURE INTERACTION SIMULATION OF SPINNAKERS – GETTING CLOSER TO REALITY

H F Renzsch, TU Delft, NL
K U Graf, University of Applied Sciences Kiel, GER

SUMMARY

This paper describes the current implementation of FlexSail, a Fluid-Structure-Interaction program for the simulation of the behaviour of spinnakers. A short outline of general membrane theory is given, the major focus lies on the impact of wrinkling and validation. A numerical modelling of anisotropic wrinkling is presented, its impact on flying shape and flow forces investigated. A newly implemented solver is described. First test cases comparing the numerical results to data from the Yacht Research Unit Kiel Twisted Flow Wind Tunnel are presented. Finally the outline of a possible optimisation algorithm for trim is shown and discussed.

NOMENCLATURE

a	scalar
$\mathbf{a}$	vector
$\mathbf{A}$	matrix
$\hat{}$	material coordinate system
$\bar{}$	element coordinate system
$\tilde{}$	wrinkled coordinate system
$_{xx}, _{yy}, _{xy}$	element axes
$_{11}, _{22}, _{12}$	material axes
$_{\varphi}$	in orientation of φ
AWA	apparent wind angle [deg]
AWS	apparent wind speed [m s^{-1}]
ε	strain
$\varepsilon_1, \varepsilon_2, \sigma_1, \sigma_2$	principal strains, stresses [N m^{-1}]
E	Young's modulus [N m^{-1}]
G	shear modulus [N m^{-1}]
$\mathbf{H}$	Hessian matrix
φ	rotation angle
m_i	virtual mass of node i
ν	Poisson number
P_{Dyn}	dynamic pressure [N m^{-2}]
$\mathbf{R}_i$	total force on node i (residual)
ρ_{Air}	density of air [kg m^{-3}]
σ	stress [N m^{-1}]
σ_m	material stress [N m^{-1}]
^{t}	at time t
$\mathbf{V}_i$	velocity of node i
$\mathbf{x}_i$	displacement of node i
y^+	dimensionless wall distance

1. INTRODUCTION

Typically, new spinnaker designs are evaluated by wind tunnel testing. Due to the problems associated with the simulation of the partially separated flow usually found around spinnakers, numerical investigation of a new design is currently still a niche application.

Simulations of the flow around sails, in particular spinnakers not only have to cope with the problem of flow separation, they also have to account for the large displacements of the sail under wind load. Thus fluid structure interaction is needed.

The historical development of Fluid-Structure-Interaction codes for the simulations of upwind sails lead to a split between structural and flow code that made sense for applications where the structural code needed the majority of the computational power. Usually the two codes where either coupled in batch mode or the structural code triggers the flow code, both codes in turn calculating until convergence individually.

These structural codes have been successfully coupled with RANSE codes in the past, yet, due to both codes calculating until convergence on each iteration, computation costs for the simulation were extremely high and practical solutions were limited to steady state.

FlexSail is a Fluid-Structure-Interaction program specifically designed to include a RANSE solver as flow code and still run in an efficient manner. To this end a different coupling paradigm, suited to the high computational costs of RANSE simulations, is used. This method is able to simulate steady state as well as fully instationary behaviour of spinnakers, capable to solve any instationarity or stability problems associated with downwind sail operation.

2. FLEXSAIL – BASIC IDEA

Like any other Fluid-Structure-Interaction program FlexSail iterates the flow and structural solver to find equilibrium in both solutions and a converged state in the coupling of both. Flow is computed using the commercial flow solver AnsysCFX 12.0, a program for the simulation of viscous flow by solving the steady or unsteady RANSE equations. The structural behaviour is simulated by a purpose-written membrane finite element code, capable of simulating large displacements and highly non-linear behaviour. It is embedded in the RANSE solver.

What sets FlexSail apart from other flow solvers is the coupling paradigm. The basic idea is to run the flow simulation in an unsteady mode. That means that each timestep is considered a valid solution. Therefore the structural code can be called from within the flow code repeatedly at given timesteps of the flow solution. See Figure 1 for a flow chart of the process.

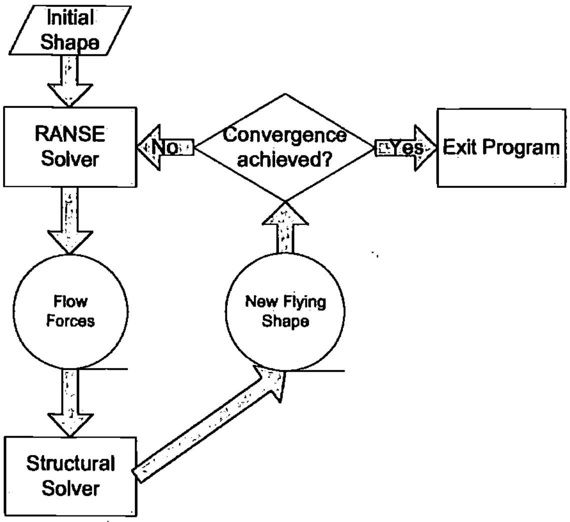

Figure 1: Flow Chart of FSI process

The coupling method (fully explicit) results in a weak two-way coupling between flow and structural simulation. Therefore the timestep length has to be significantly smaller than any natural periods of dynamic occurrences considered in dynamic simulations. A typical application is shown in [1].

3. BASIC MEMBRANE THEORY

3.1 GENERAL

Generally the stress – strain relationship is given by:

$$\boldsymbol{\sigma} = \mathbf{H} \cdot \boldsymbol{\varepsilon}$$

with $\boldsymbol{\varepsilon} = \left\{\varepsilon_{xx}; \varepsilon_{yy}; \sqrt{2}\varepsilon_{xy}\right\}^T$ and $\boldsymbol{\sigma} = \left\{\sigma_{xx}; \sigma_{yy}; \sqrt{2}\sigma_{xy}\right\}^T$. The factor $\sqrt{2}$ is included just for mathematical convenience later on.

To discretise the sail, Constant Stress Triangle elements as described in Figure 2 are used.

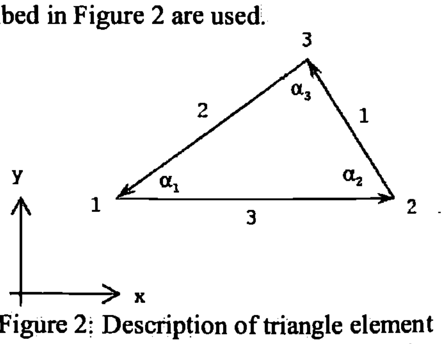

Figure 2: Description of triangle element
Note that edge 3 is parallel to the x-axis.

In FlexSail linear Hookean materials are assumed. The generalised stress-strain relationship, the Hessian matrix $\hat{\mathbf{H}}$, for the linear behaviour of an arbitrary material in material coordinate system 1-2 (see Figure 3) is the partial derivative of stress by strain and can be written as:

$$\hat{\mathbf{H}} = \begin{bmatrix} \frac{\partial\sigma_{11}}{\partial\varepsilon_{11}} & \frac{\partial\sigma_{11}}{\partial\varepsilon_{22}} & \frac{\partial\sigma_{11}}{\partial\varepsilon_{12}} \\ \frac{\partial\sigma_{22}}{\partial\varepsilon_{11}} & \frac{\partial\sigma_{22}}{\partial\varepsilon_{22}} & \frac{\partial\sigma_{22}}{\partial\varepsilon_{12}} \\ \frac{\partial\sigma_{12}}{\partial\varepsilon_{11}} & \frac{\partial\sigma_{12}}{\partial\varepsilon_{22}} & \frac{\partial\sigma_{12}}{\partial\varepsilon_{12}} \end{bmatrix}$$

This approach only holds true under the assumption of small strains. In case of large strains non-linear coupling effects have to be included in a fourth stage tensor.

The stress strain relations for arbitrary directions, where the material directions have been rotated a positive angle φ from the x-axis (see Figure 3), can be written as follows:

$$\overline{\boldsymbol{\sigma}} = \mathbf{T}^{-1} \cdot \hat{\mathbf{H}} \cdot \mathbf{T} \cdot \overline{\boldsymbol{\varepsilon}}$$

With $\mathbf{T}$ being the transformation matrix from element to material coordinate system:

$$\mathbf{T} = \begin{bmatrix} c^2 & s^2 & \sqrt{2}cs \\ s^2 & c^2 & -\sqrt{2}cs \\ -\sqrt{2}cs & \sqrt{2}cs & c^2 - s^2 \end{bmatrix}$$

$$c = \cos(\varphi);\ s = \sin(\varphi).$$

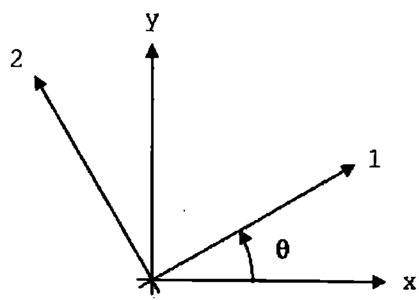

Figure 3: Element and material coordinate systems

A more detailed description of the structural method is given in [2] and [3].

4. ANISOTROPIC WRINKLING

A significant shortcoming of the basic membrane stress – strain formulation is its behaviour under compressive in-plane loads. "Real" sailcloth has a negligible bending stiffness and therefore negligible buckling strength, with compressive in-plane loads causing the cloth to wrinkle. Unfortunately, the basic membrane formulation has the same stress-strain gradient under compression as well as under tension.

This shortcoming is corrected by using a wrinkling model. Basic wrinkling models [4], [5] alter the stiffness matrix in case of wrinkling, yet until now this has only been described for isotropic materials and, in fact, doesn't replicate the real behaviour of materials. Other wrinkling models [6], [7] modify the deformation vector under following observations:

- A wrinkled membrane is in a state of uniaxial tension.
- The wrinkles are aligned with this uniaxial tension.
- Material stresses are invariant to strain changes perpendicular to the wrinkles as long as the membrane is not coming under tension in this direction.
- In anisotropic materials principal stresses and strains are not aligned.
- If we assume the taut state as a starting point and reduce principle stress in direction two (σ_2), the basic membrane formulation holds up to - and including - the point where σ_2 is exactly zero but the material not yet wrinkled. From this point on material stress remains unchanged while element strain changes further (this assuming principle stress σ_1 being greater or equal than principle stress σ_2)

These observations lead to the mixed stress – strain wrinkling criterion

$$\begin{aligned}&\sigma_2 > 0 \Rightarrow \textit{taut}\\ &\varepsilon_1 \le 0 \Rightarrow \textit{slack}\\ &\varepsilon_1 > 0 \textit{ and } \sigma_2 \le 0 \Rightarrow \textit{wrinkled}\end{aligned}$$

and following modification of the membrane formulation assuming uniaxial tension in direction φ:

$$\boldsymbol{\sigma}_m^\varphi = \mathbf{H}^\varphi \cdot \left(\boldsymbol{\varepsilon}^\varphi + \boldsymbol{\varepsilon}_w^\varphi\right)$$

with the material stress $\boldsymbol{\sigma}_m^\varphi = \begin{Bmatrix}\sigma_{m11}^\varphi\\ 0\\ 0\end{Bmatrix}$

and the wrinkling strain $\boldsymbol{\varepsilon}_w^\varphi = \begin{Bmatrix}0\\ \varepsilon_{w22}^\varphi\\ 0\end{Bmatrix}$, where $\varepsilon_{w22}^\varphi$ is a measure for the amount of wrinkling.

Geometrically this modification can be described as shown in Figure 4:

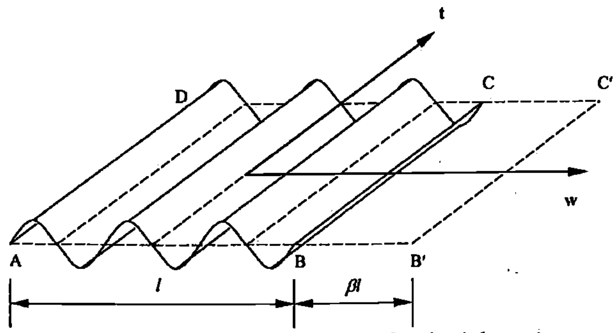

Figure 4: material under *natural* uniaxial tension (AB'C'D) and uniaxial tension (wrinkled, ABCD) [5]

ABCD are the corners of a wrinkled membrane element under uniaxial tension in direction **t**. Material stress in direction **w** is zero, yet strain in direction **w** is negative finite. If we extend the membrane direction **w** exactly up to the point where the wrinkles vanish but material stress is still zero (AB'C'D), we find the state of *natural* uniaxial tension. Up to this state material stress is invariant, yet from this state on the regular membrane formulation holds true.

In the state of *natural* uniaxial tension we can write:

$$\boldsymbol{\sigma}_m^\varphi = \mathbf{H}^\varphi \cdot \boldsymbol{\varepsilon}^\varphi$$

Defining $\boldsymbol{\sigma}_m^\varphi = \{\sigma_{m11}^\varphi;0;0\}^T$ we can rewrite:

$$\varepsilon_{22}^\varphi = \frac{H_{21}^\varphi H_{33}^\varphi - H_{23}^\varphi H_{31}^\varphi}{H_{23}^\varphi H_{32}^\varphi - H_{22}^\varphi H_{33}^\varphi} \cdot \varepsilon_{11}^\varphi$$

and

$$\varepsilon_{12}^\varphi = \frac{H_{22}^\varphi H_{31}^\varphi - H_{21}^\varphi H_{32}^\varphi}{H_{23}^\varphi H_{32}^\varphi - H_{22}^\varphi H_{33}^\varphi} \cdot \varepsilon_{11}^\varphi$$

Under the observations above we now can state that the formulation for ε_{12}^φ holds true for general uniaxial tension, while ε_{22}^φ is restricted to *natural* uniaxial tension.

Now we have two ways of calculating $\boldsymbol{\varepsilon}^\varphi$:

- from rotation $\breve{\boldsymbol{\varepsilon}}^\varphi = \mathbf{T} \cdot \boldsymbol{\varepsilon}$
- $\hat{\boldsymbol{\varepsilon}}^\varphi$ from the conditions for *natural* uniaxial tension given above

Given the two methods to determine $\boldsymbol{\varepsilon}$, now we have to numerically find the angle φ where, under the condition of $\hat{\varepsilon}_{11}^\varphi = \breve{\varepsilon}_{11}^\varphi$, ε_{11} is positive definite, $\hat{\varepsilon}_{12}^\varphi = \breve{\varepsilon}_{12}^\varphi$ and $\hat{\varepsilon}_{22}^\varphi \ge \breve{\varepsilon}_{22}^\varphi$. $\varepsilon_{w22}^\varphi$ is given by $\varepsilon_{w22}^\varphi = \hat{\varepsilon}_{22}^\varphi - \breve{\varepsilon}_{22}^\varphi$ and is always positive finite.

5. SOLVER

The solver used so far for the structural part of FlexSail was based based on the minimization of total potential energy using a modified Newton approach [2]. However it was not able to treat the strong structural nonlinearities associated with wrinkling. Thus a new solver has been implemented.

Promising the necessary stability, a kinetically damped *Dynamic Relaxation* approach was chosen to solve the finite-element case [8]. In this approach separate equations for equilibrium and compatibility are used. The structure is described by a dampened vibrating system with virtual masses on the nodes and link forces to describe the elements. The solution then is based on a time strepping scheme.

Basically the motion of any node i at time t can be described by Newton's 2nd law of motion as

$$\dot{\mathbf{V}}_i^t = \frac{\mathbf{R}_i^t}{m_i}$$

with $\mathbf{R}_i^t$ being the vectorial sum of all forces (internal and external) acting on node i at time t.

In centred difference form this acceleration term can be approximated as:

$$\dot{\mathbf{V}}_i^t = \frac{\mathbf{V}_i^{t+\Delta t/2} - \mathbf{V}_i^{t+\Delta t/2}}{\Delta t}.$$

This yields the following term for nodal velocities at time $(t+\Delta t/2)$:

$$\mathbf{V}_i^{t+\Delta t/2} = \mathbf{V}_i^{t+\Delta t/2} + \Delta t \cdot \frac{\mathbf{R}_i^t}{m_i}$$

The updated geometry projected to time $(t+\Delta t)$ is therefore given by:

$$\mathbf{x}_i^{t+\Delta t} = \mathbf{x}_i^t + \Delta t \cdot \mathbf{V}_i^{t+\Delta t/2}$$

The virtual masses used above are calculated by

$$m_i = \frac{\Delta t^2}{2} \cdot S_i$$

With S_i being the largest direct stiffness that may occur during analysis.

To get the dynamic relaxation solver to converge some kind of damping method is necessary. Typically used is either viscous or kinetic damping. For FlexSail kinetic damping was chosen as it gives robust performance with little computational overhead. In a kinetically damped system kinetic energy peaks of the whole vibrating system are detected and all nodal velocities set to zero before releasing the nodes again.

Due to the separation of equilibrium and compatibility giving a vectorial formulation of the problem, no global stiffness matrix has to be constructed, keeping computational overhead low. The vectorial formulation lends itself to parallelising using a SPMD paradigm on a multi-core machine.

6. IMPACT OF WRINKLING

Wrinkling has a dramatic impact on the shape of the sail. As shown in [9] for sails with little Gaussian deformation the amount of draft and its position is significantly changed. On sails with significant Gaussian deformation the impact is even more dramatic.

To show the effects flying shapes under constant pressure difference were calculated for a symmetric spinnaker with significant tack displacement and sheet length change. In Figure 5 the designed shape of the investigated spinnaker is shown. For discretization a triangular net of 7250 elements is used.

Figure 6 gives the flying shapes without and with wrinkling model.

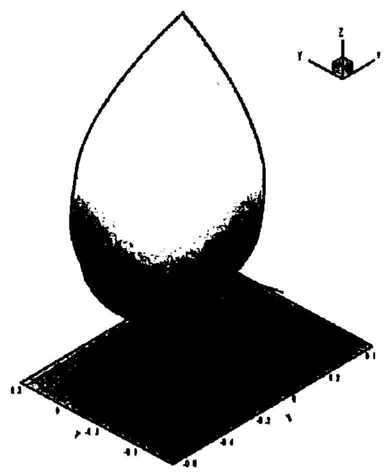

Figure 5: Mould of tested spinnaker (design shape)

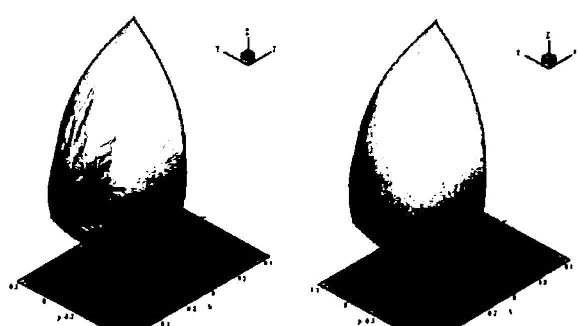

Figure 6: Flying shapes without (left) and with (right) wrinkling model

It can be seen that without accounting for wrinkling (Figure 6, left), significant folds radiate from the tack. Under strong Gaussian deformations the membrane without wrinkling model appears to behave like a thin sheet of plastic or metal under compression. Figure 6, right does not show this behaviour. Wrinkling is not visible as it occurs on a sub-element scale.

Figures 7 and 8 show principle stresses in direction 1 and 2. With wrinkling model the principal stresses 1 mostly radiate out from the corners and go up the side leeches, dissipating towards the centre of the sail. Principal stresses 2 are oriented perpendicular to them and equal or larger than zero. Without wrinkling model the principal stresses 1 are primarily oriented along the folds with significantly negative principal stresses 2 across the folds.

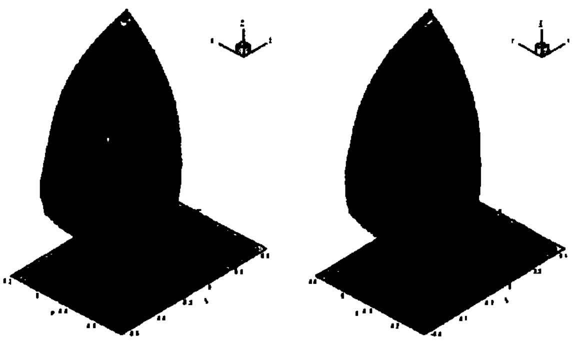

Figure 7: Principle stress 1 without and with wrinkling model

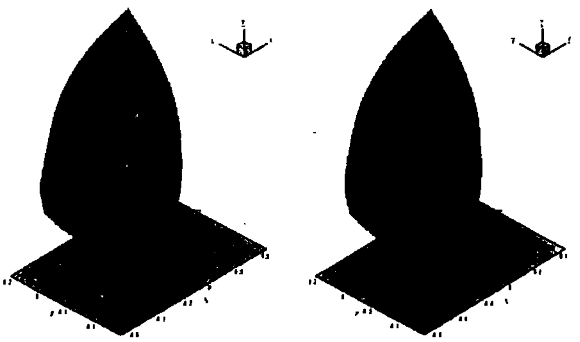

Figure 8: Principle stress 2 without and with wrinkling model

7. INITIAL TESTCASES

To get a first comparison between simulation and experimental results, wind tunnel tests with sail shape capturing were conducted at the YRU-Kiel Twisted Flow Wind Tunnel.

7.1 WIND TUNNEL TESTING

A symmetric spinnaker was tested in the Yacht Research Unit Kiel's Twisted Flow Wind Tunnel (TFWT) [3]. This spinnaker was the result of a development for sailmakers *Holm Segel Schleswig/Germany.* The spinnaker design was developed as a generic mould based on a 40' cruiser/racer. During the tests it emerged to be beneficial to trade area for a more stable and controllable shape, maintaining more attached flow over a wider range of *AWA*s. Therefore the spinnaker has less than maximum area within the given design envelope. During wind tunnel tests the final design has proven to be quite stable and forgiving while having driving forces comparable to maximum sized spinnakers at significantly reduces sideforces. This is corroborated by initial impressions during testing this spinnaker at full scale.
The spinnaker was tested over an AWA-range of 67.5° to 180° at an *AWS* of 5 m s^{-1}. Trim settings were recorded during the tests for use in simulations. The test results are given in Figure 9, reproducibility of the results were confirmed during tests measurements using the recorded trim settings. For scaling and comparison purposes the forces are normalized by the dynamic pressure of the apparent wind ($P_{Dyn} = 1/2 \cdot \rho_{Air} \cdot AWS^2$), resulting in force areas.

The general arrangement of the TFWT is shown in Figure 10.

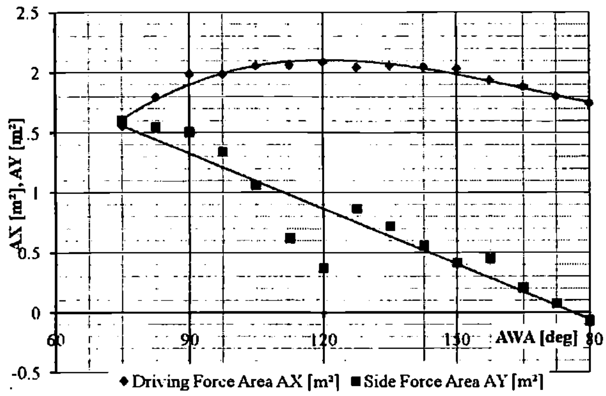

Figure 9: Driving and side force areas for spinnaker and main from TFWT-measurements

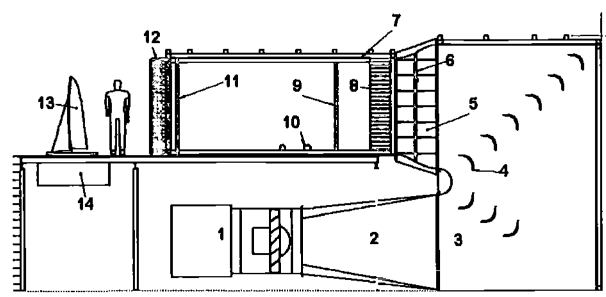

Figure 10: General arrangement of YRU-Kiel Twisted Flow Wind Tunnel

7.1 (a) Flying shape capturing

During the TFWT measurements the flying shape of main sail and spinnaker was recorded using photogrammetric techniques [10]. Figure 11 shows the relation between an exemplary picture used for the measurements and the resulting CAD model. The images were processed using *Photomodeller®*.

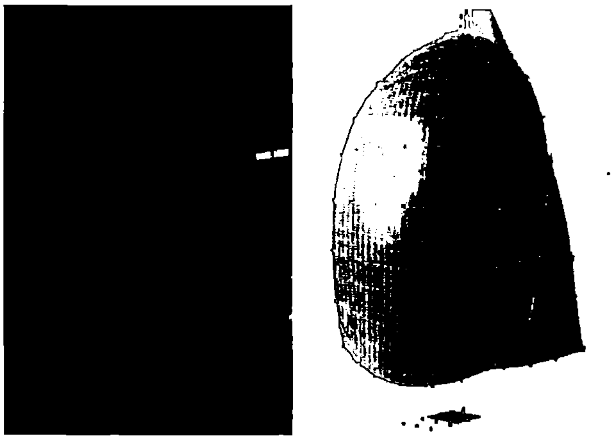

Figure 11: Exemplary photo from photogrammetric measurements and corresponding CAD model

7.2 FIRST SIMULATIONS

The spinnaker and main sail as tested in the TFWT were simulated using FlexSail at a few selected apparent wind angles. The incident flow conditions were modelled to approximate the wind tunnel incident flow. Trim settings were taken from the wind tunnel measurements. The simulations were carried out at model scale to keep Reynold's-similarity. The main sail was set fixed to the trim recorded in the TFWT.

A computational grid of 2.26m volume elements with boundary layer refinement around sails and hull was used for the CFD calculations. The spinnaker was discretised using 7250 triangular elements for the structural calculations. Typically y^+ is within the range of 15 to 20. Total runtime on 18 CPU-cores was 3:20h.

The spinnaker has following dimensions:

SL [m] =	1.43
SMG [m] =	0.766
SF [m] =	0.808
Area [m²] =	0.923

Figure 12 shows the design output from the sailmaker's lofting program *ProSail.*

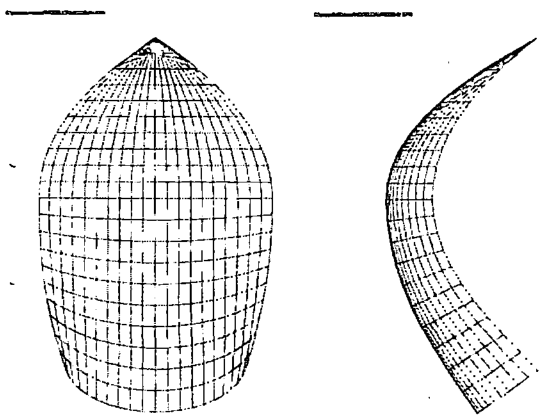

Figure 12: Designed shape from *ProSail*

The result of the simulation shows a significant change from designed shape to flying shape, Figure 13 compares design and flying shape at $AWA = 90°$.

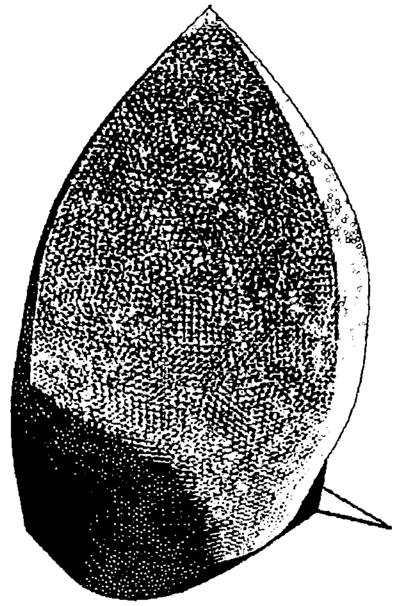

Figure 13: Designed (grey) and computed flying (black) shape at AWA = 90°

It can be seen that the flying shape shows a quite significant change of distance between tack and head compared to the designed shape (as well apparent in the investigation on the effect of wrinkling). Combined with the change of sheet length this leads to significant displacement compared to the designed shape.

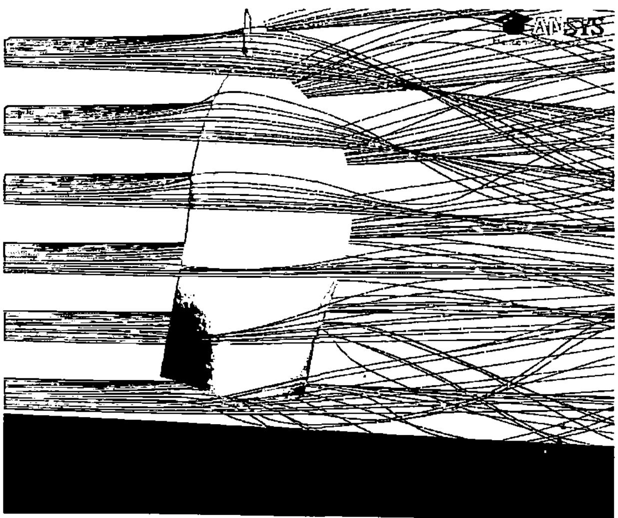

Figure 14: Streamlines around boat and sails

The streamlines in Figure 14 show clean flow behaviour around the body of the spinnaker. Only near head, foot and close to the leech some divergence of the streamlines is visible, indicating separation in these areas. This is supported by the pressure distribution shown in Figure 15. Near the luff an area of low pressure can be observed indicating a suction peak. The interruption of this area close to mid-luff indicates a locally non-optimum luff twist distribution. The pressure increases gradually towards the leech.

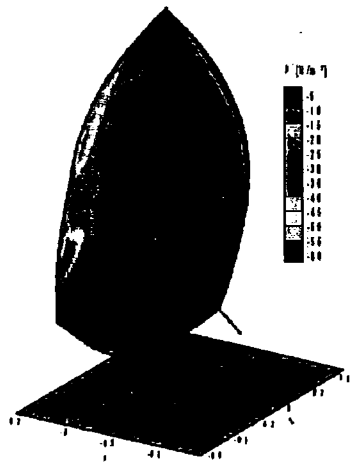

Figure 15: Pressure distribution on spinnaker

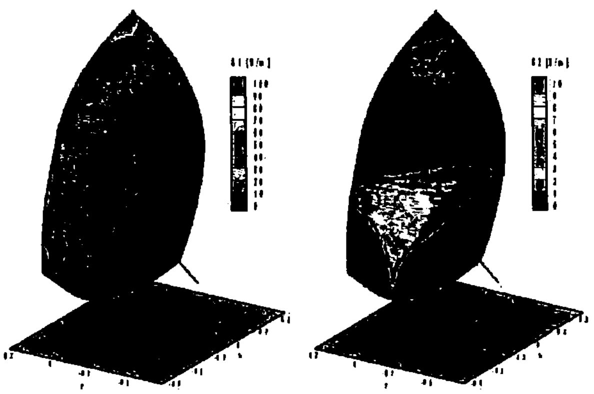

Figure 16: Principal stresses in directions one and two

Figure 16 shows the distributions of principal stresses (σ_1 and σ_2) within the spinnaker. It is clearly observable that the largest stresses (areas of large σ_1) run up the luff. σ_2 is zero in large parts of the sail, yet, as the sail's size is not visibly reduced, the cloth in these areas appears to be right at the verge of wrinkling. Near the head σ_2 is larger than zero, indicating that the behaviour of the sail near the head will be quite stable. This is supported by observations during trimming in the TFWT.

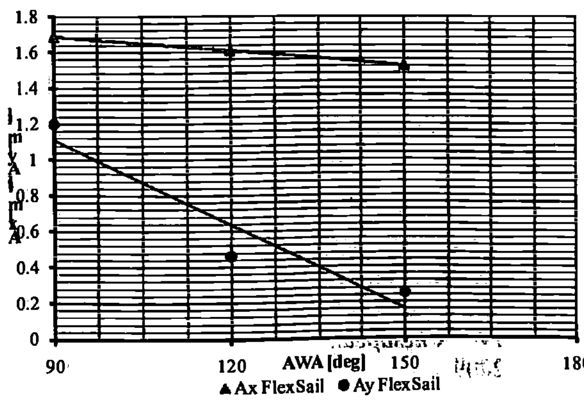

Figure 17: Force areas of sail set

Figure 17 gives driving and sideforce areas calculated by FlexSail for three selected *AWA*s.

7.3 COMPARISION

To evaluate the quality of the simulations, flying shapes and forces from TFWT measurements and simulations have to be compared.

The comparison of the flying shapes (Figure 18) shows very close agreement. The slight deviations near the head can be explained by scaling errors of the measured flying shape. The deviation of the foot is due to having to reconstruct the CAD-geometry of the designed shape as *ProSail* unfortunately has no directly usable output of the mould / designed shape.

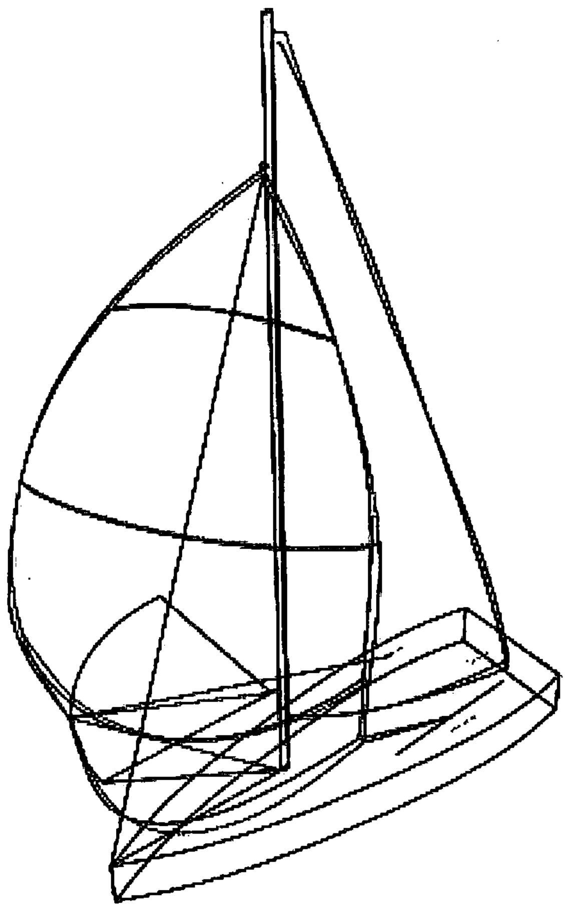

Figure 18: Comparison of measured (dashed) and computed (continuous) flying shape

Figure 19 gives a comparison of the force areas from TFWT tests and simulations. While the same general trend is discernible there is a significant offset both in driving as in side force area. To date no explanation for this offset is known, further investigations are in progress.

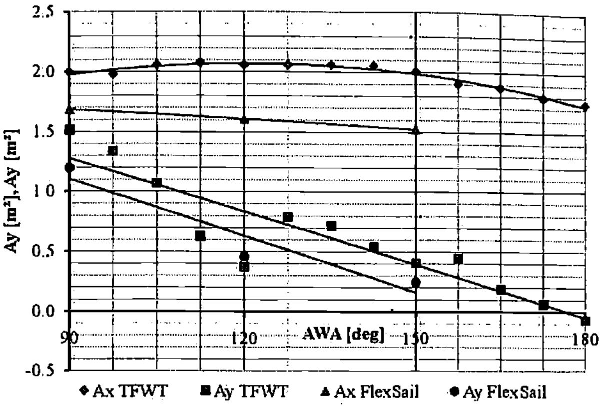

Figure 19: Force areas from TFWT measurements and simulations

8. OPTIMISER

In the wind tunnel and while sailing in a race the sail trimmer constantly alters the trim settings of the sail to optimize driving force respectively boat speed. For proper simulation a method mimicking this behaviour has to be included within the FSI program.

A constraint optimiser for inclusion into FlexSail is currently under development. Due to the amount of computational resources needed, the optimiser does not target sail design but trim optimisation. The current aim is to optimise one or two trim variables with the challenge being to be as economical with computational resources as possible. In the initial version the sheet length of an asymmetric spinnaker will be changed, looking for maximum driving force. Later on sheet lead position or tack line length are possible additional candidates for optimisation.

The challenge in the development of the optimiser is to get a higher throughput than by permutating trim settings in a batch job while maintaining stability of the solution.

9. CONCLUSIONS

The development of a program for the simulation of the flow around and the structural behaviour of downwind sails has been described. A physically correct wrinkling model has been detailed, a short overview of solver, stable even at large geometrical as well as structural non-linearities, has been given. Results from TFWT-tests including photogrammetric measurements and corresponding simulations are shown. A comparison indicates extremely good geometric agreement. The force deviations require further investigations. First thoughts on the development of an automatic trim optimiser for the simulations are given.

Short term work focuses on finding and rectifying the force offset between TFWT and simulation results. For this investigation the simulation as well as the wind tunnel test results will have to be scrutinised. Further development work will be the implementation of the trim optimiser as sketched above and the parallelisation of the FE-solver. Those two measures offer the potential to significantly reduce runtime per case as well as per trim series for a given sail and AWA.

10. REFERENCES

1. GRAF, K., BÖHM, C., RENZSCH, H., 'CFD- and VPP-Challenges in the Design of the New AC90 Americas Cup Yacht', *Proceedings 19th Chesapeake Sailing Yacht Symposium*, 2009

2. GRAF, K., RENZSCH, H., 'RANSE Investigations of Downwind Sails and Integration into Sailing Yacht Design Processes', *Proceedings 2nd High Performance Yacht Design Conference*, 2006

3. RENZSCH, H., MÜLLER, O., GRAF, K., 'FlexSail – A Fluid Structure Interaction Program for the Investigation of Spinnakers', *Proceedings Innov'Sail*, 2008

4. MILLER, R. K., HEDGEPETH, J. M., 'An Algorithm for Finite Element Analysis of Partially Wrinkled Membranes', *AIAA Technical Note 82-4293*, 1982

5. ADLER, A. L., MIKULAS, M. M., HEDGEPETH, J. M., 'Static and Dynamic Analysis of Partially Wrinkled Membrane Structures', *AIAA-2000-1810*, 2000

6. KANG, S., IM, S., 'Finite Element Analysis of Wrinkling Membranes', *Journal of Applied Mechanics, Vol. 64*, 1997

7. LU, K., ACCORSI, M., LEONARD, J., 'Finite Element Analysis of Membrane Wrinkling', *International Journal for Numerical Methods in Engineering, 50*, 2001

8. BARNES, M. R., 'Form Finding and Analysis of Tension Structures by Dynamic Relaxation', *International Journal of Space Structures Vol. 14 No. 2*, 1999

9. HEPPEL, P., 'Accuracy in Sail Simulation: Wrinkling and growing fast sails', *Proceedings High Performance Yacht Design Conference*, 2002

10. GRAF, K., MÜLLER, O., 'Photogrammetric Investigation of the Flying Shape of Spinnakers in a Twisted Flow Wind Tunnel', *Proceedings 19th Chesapeake Sailing Yacht Symposium*, 2009

11. AUTHORS' BIOGRAPHIES

HANNES RENZSCH holds a diploma degree in naval architecture from the University of Applied Sciences Kiel. He works as a scientist at the Yacht Research Unit Kiel. Hannes specialises in numerical and experimental aerodynamics and corresponding software development. He is responsible for wind tunnel testing at the Yacht Research Unit Kiel's Twisted Flow Wind Tunnel. Hannes is currently working towards his PhD-at TU Delft.

KAI GRAF is professor for ship hydrodynamics at the University of Applied Sciences Kiel and senior scientists of the Yacht Research Unit Kiel. Kai is working on sailing yacht aero- and hydrodynamics since 1998, specialising in numerical simulation methods.